Longitudinal Proximity Effects in Superconducting Transition-Edge Sensors

John E. Sadleir,[1,2,*] Stephen J. Smith,[2] Simon R. Bandler,[2] James A. Chervenak,[2] and John R. Clem[3]

[1]*Department of Physics, University of Illinois, 1110 West Green Street, Urbana, IL 61801-3080*
[2]*NASA Goddard Space Flight Center, 8800 Greenbelt Road, Greenbelt, MD 207701*
[3]*Ames Laboratory and Department of Physics and Astronomy, Iowa State University, Ames, Iowa, 50011-3160*

(Dated: December 22, 2009)

We have found experimentally that the critical current of a square thin-film superconducting transition-edge sensor (TES) depends exponentially upon the side length L and the square root of the temperature T, a behavior that has a natural theoretical explanation in terms of longitudinal proximity effects if the TES is regarded as a weak link between superconducting leads. As a consequence, the effective transition temperature T_c of the TES is current-dependent and at fixed current scales as $1/L^2$. We also have found that the critical current can show clear Fraunhofer-like oscillations in an applied magnetic field, similar to those found in Josephson junctions. We have observed the longitudinal proximity effect in these devices over extraordinarily long lengths up to 290 μm, 1450 times the mean-free path.

PACS numbers: 74.25.-q,74.78.Bz,74.25.Op

A superconductor cooled through its transition temperature T_c while carrying a finite dc bias current undergoes an abrupt decrease in electrical resistance from its normal-state value R_N to zero. Superconducting transition-edge sensors (TESs) exploit this sharp transition; these devices are highly sensitive resistive thermometers used for precise thermal energy measurements.[1] Various models[2–6] have been used to explain the noise, T_c, and transition width ΔT_c in TESs, all assuming spatially uniform devices. Though some have been shown to be consistent with certain aspects of particular devices, they do not explain measured T_c and ΔT_c in TESs generally. In this paper we emphasize the importance of a phenomenon that so far has been neglected in previous theoretical studies of TESs: the longitudinal proximity effect (LoPE). The square superconducting/normal-metal (S/N) bilayers at the heart of the TES have an intrinsic transition temperature T_{ci} without leads attached. However, since the bilayers are connected at opposite ends to superconducting leads with transition temperatures well above T_{ci}, superconductivity is induced longitudinally into the bilayers from the ends via the proximity effect, Fig. 1. As we shall explain later, many of the basic properties of our TES structures are well described by regarding them as SS′S or SN′S weak links.[7–9]

This observed long-range longitudinal proximity effect also contributes to the basic understanding of S/N heterostructures more broadly. Supercurrents have been measured through S/N/S sandwiches over N thicknesses D as long as 40 μm.[10] In these pioneering experiments by Shepherd the clean normal metal (rolled Cu foils) has mean free paths $\ell \approx 16$ μm giving a $D/\ell \approx 2.5$. In contrast we present measurements on SN′S films well described by our proximity effect model with N′ lengths L from 8 to 290 μm with normal-state mean-free paths $\ell \approx$ 200 nm giving L/ℓ ratios of 40 to 1450.

Despite poor understanding of the physics governing TESs biased in the superconducting phase transition, significant strides have been made in sensor development.[1] TES microcalorimeters have been developed with measured energy resolutions in the x-ray and gamma-ray band of $\Delta E = 1.8 \pm 0.2$ eV FWHM at 6 keV,[11] and $\Delta E = 22$ eV FWHM at 97 keV,[12] respectively—with the latter result at present the largest reported $E/\Delta E$ of any non-dispersive photon spectrometer. TESs are successfully used across much of the electromagnetic spectrum, measuring the energy of single-photon absorption events from infrared to gamma-ray energies and photon fluxes out to the microwave range.[1] There are active TES research and development programs underway in many physics fields for materials microanalysis,[13] mass spectroscopy of biomolecules,[14] nuclear nonproliferation,[12] synchrotron experiments,[15] atomic physics,[16] quantum information,[17,18] dark-matter searches,[19] and astrophysics,[1] including future large-scale

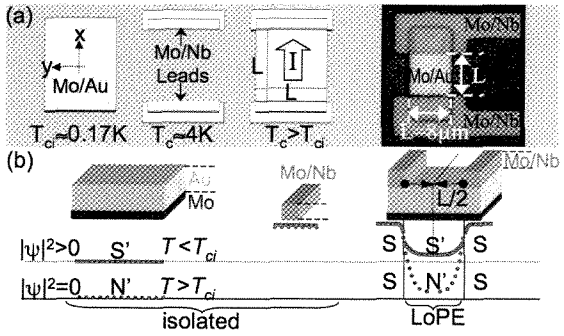

FIG. 1: (Color available online) Figure (a) from left to right shows a Mo/Au bilayer to which Mo/Nb leads are added of separation L (the current I flows from lead to lead) and a picture of the $L = 8$ μm sample. (b) Schematic showing the modulus squared of the order parameter $|\psi|^2$ for temperatures above (dotted line) and below (solid line) T_{ci}. Far right schematic shows the spatial variation of $|\psi|^2$ enhanced in the Mo/Au due to the Mo/Nb leads.

NASA space-based cosmic microwave background[20] and x-ray imaging-spectroscopy observatories.[21]

To achieve high energy resolution it is important to control both the TES's T_c and ΔT_c. Because the energy resolution of calorimeters improves with decreasing temperature, they are typically designed to operate at temperatures around 0.1 K. For a TES, this requires a superconductor with T_c in that range. While there exist a few suitable elemental superconductors, the best results have been achieved using proximity-coupled, S/N bilayers[11,12], for which T_c is tuned by selection of the thicknesses of the S and N layers.[2]

We report here the properties of TESs based on square ($L \times L$) electron-beam-deposited Mo/Au bilayers consisting of a 55 nm Mo layer ($T_c \sim 0.9$ K) to which 210 nm of Au is added. The square side lengths L range from 8 μm to 290 μm, and the normal-state resistance per square is $R_N = 17.2 \pm 0.5$ mΩ. The bilayers are connected at opposite ends to Mo/Nb leads having measured superconducting transition temperatures of 3.5 and 7.1 K.[22] Further details on the device fabrication process can be found in Ref. 23.

Our measurements are made in an adiabatic demagnetization refrigerator (ADR) with mu-metal and Nb enclosures providing magnetic shielding for the TES devices and SQUID electronics. The magnetic field normal to the TES device plane is controlled by a superconducting coil with the field value determined from the coil geometry and current. Measurements of the TES resistance R are made by applying a sinusoidal current of frequency 5-10 Hz and amplitude $I_{bias} \sim$ 50-250 nA, with zero dc component, to the TES in parallel with a 0.2 mΩ shunt resistor (R_{sh}). The time-dependent TES current is measured with a SQUID feedback circuit with input coil in series with the TES. When I_{bias} is less than the TES critical current I_c, R is zero, and all the ac current flows through the TES. However, when $I_{bias} > I_c$ and $R > 0$ during part of the ac cycle, the TES current becomes non-sinusoidal, and its maximum value I becomes less than I_{bias}. The TES resistance R at the TES current I is then determined from $R = R_{sh}(I_{bias} - I)/I$.

The critical current I_c is measured, with the ADR held at constant temperature, by ramping the dc bias current from zero and defining I_c as the TES current at the first measured finite resistance ($R \sim 10$ $\mu\Omega$) across the TES. Record averaging is used at higher temperatures where I_c becomes small.

The solid curves in Fig. 2 show measurements of the critical current I_c over seven decades vs temperature T. Note that although we find the intrinsic transition temperature of the Mo/Au bilayer is $T_{ci} = 170.9 \pm 0.1$ mK, at very low currents a zero-resistance state is measured up to much higher temperatures as the TES size is reduced, three times T_{ci} for $L = 8$ μm. On the other hand, for the larger TES sizes (L=130 and 290 μm) the critical current $I_c(T)$ decreases rapidly with T near T_{ci}. The observed I_c behavior as functions of both T and the length L provides strong evidence that our TESs behave as weak-link devices. The dotted curves in Fig. 2 show calculated values of I_c using the Ginzburg-Landau theory described below. In addition, at appropriately chosen temperatures, the critical currents of these devices exhibit Fraunhofer-like oscillations as a function of an applied magnetic field, behavior characteristic of Josephson weak links.[8,24] See Fig. 3 for an example. However, the spacing between the minima corresponds to a junction magnetic flux of approximately BL^2, similar to the spacing predicted in Ref. 25 for edge-type Josephson junctions in thin-film strips.

Because I_c depends upon T and L, the effective tran-

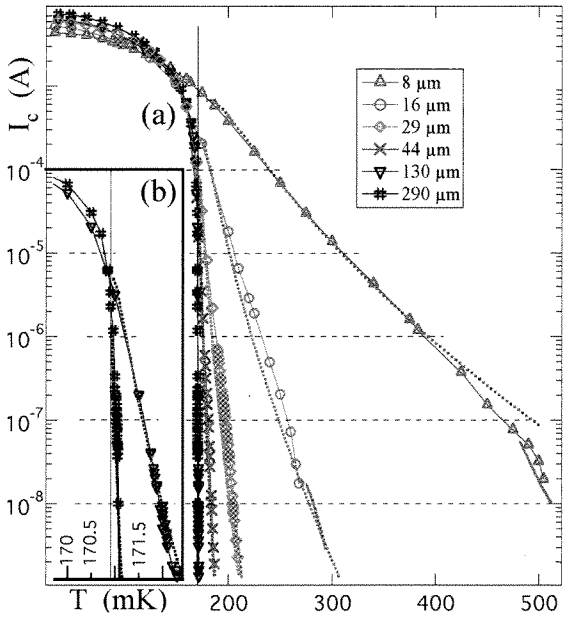

FIG. 2: Figure (a) and inset (b) show measured (solid lines and markers) and theoretical (dotted curves) critical current I_c versus temperature T for square TESs with side lengths L ranging from 8 to 290 μm. The bold continuous segments at the lowest currents are obtained by record averaging. The intrinsic transition temperature of the Mo/Au bilayer weak links is $T_{ci} = 170.9 \pm 0.1$ mK (thin vertical lines). T and L values of the constant current contours (horizontal dashed lines) are plotted in Fig. 4(a).

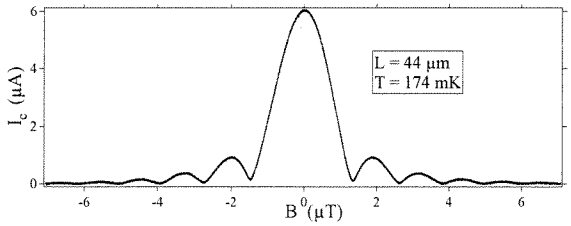

FIG. 3: I_c vs applied field for the $L = 44$ μm device showing Fraunhofer-like oscillations, similar to those seen in Josephson junctions, providing further evidence that the TES exhibits weak-link behavior.

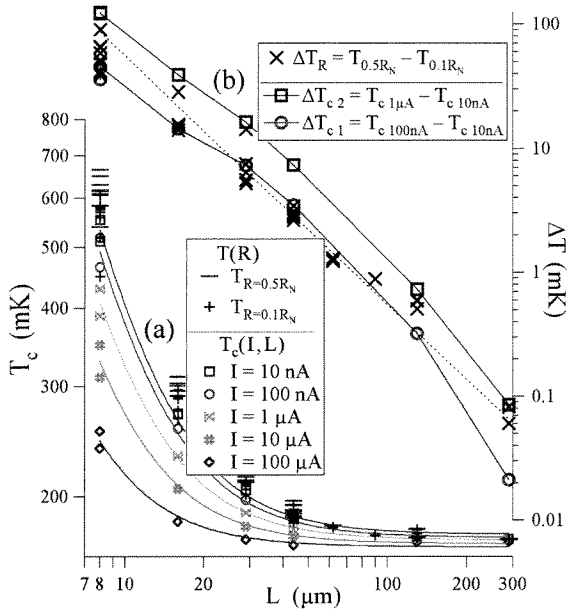

FIG. 4: (a) Measurements of the effective transition temperature T_c at different currents and lengths. Markers $T_c(I,L)$ give the effective T_c from constant current contours of the $I_c(T,L)$ data in Fig. 2, with solid curves being $1/L^2$ fits for each current level. Markers $T(R)$ give temperatures where $R = 0.1\,R_N$ and $0.5\,R_N$. (b) Three different measures of the transition width defined as differences between pairs of corresponding points shown in (a), as labeled ΔT_R, $\Delta T_{c\,1}$, and $\Delta T_{c\,2}$, showing $1/L^2$ scaling (dotted line).

sition temperature T_c of the TES (the temperature at which an electrical resistance first appears, i.e., $R \sim 10\ \mu\Omega$) is both current-dependent and length-dependent. Figure 4(a) exhibits these effects. The points labeled $T_c(I,L)$ are the effective transition temperatures at five different current levels (10 nA to 100 μA) for the data in Fig. 2, showing that $T_c - T_{ci}$ for each current level scales approximately as $1/L^2$ (solid curve fits) for L ranging from 8 to 290 μm. For each L, $T_c - T_{ci}$ depends upon the current.

Also shown in Fig. 4(a) are temperatures $T_{R=0.1\,R_N}$ and $T_{R=0.5\,R_N}$ for which the resistances are $R = 0.1\,R_N$ and $0.5\,R_N$, respectively, from which we define $\Delta T_R = T_{0.5R_N} - T_{0.1R_N}$. We also define transition widths from the I_c measurements $\Delta T_{c\,1} = T_{c\,100nA} - T_{c\,10nA}$ and $\Delta T_{c\,2} = T_{c\,1\mu A} - T_{c\,10nA}$. In Fig. 4(b) we show that these three measures of the transition width all vary approximately as $1/L^2$, shown by the dotted line. It also follows that $T_c - T_{ci}$ scales linearly with the transition width.

Weak links have been studied experimentally and theoretically by numerous authors. However, here we use a simple version of Ginzburg-Landau (GL) theory, which will be described in more detail elsewhere, to explain the results shown in Figs. 2 and 4. The calculations yield the

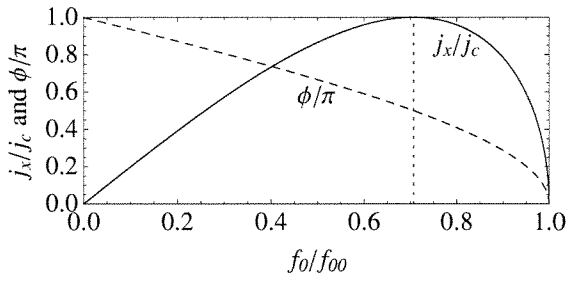

FIG. 5: Critical current density j_x (solid, in units of j_c) and gauge-invariant phase difference ϕ (dashed, in units of π) vs f_0/f_{00} from Eq. (1) when $T > T_{ci}$ and $L \gg \xi(T)$. Along the vertical dotted line at $f_0/f_{00} = 1/\sqrt{2}$, $j_x = j_c$ and $\phi = \pi/2$.

normalized order parameter $f = |\psi|/\psi_r$, where ψ_r is the magnitude of the order parameter at the reference points $x = \pm L/2$ adjacent to the leads. At the reference points, the local value of ψ_r^2 is related to the local penetration depth λ_r via $\psi_r^2 = m/4\mu_0 e^2 \lambda_r^2$. There is a second characteristic length in GL theory, the temperature-dependent coherence length $\xi(T) = \xi_i/|t-1|^{1/2}$, where T is the absolute temperature, T_{ci} is the intrinsic transition temperature of the weak link in the absence of leads, and $t = T/T_{ci}$ is the reduced temperature.

Near the center of the weak link, where f becomes very small, the local penetration depth $\lambda = \lambda_r/f$ becomes very large. Moreover, in a thin film of thickness $d < \lambda$, magnetic fields and currents spread out over the two-dimensional screening length (or Pearl length[26]) $\Lambda = 2\lambda^2/d = 2\lambda_r^2/df^2$. For all of our samples there is a range of temperatures T far enough above T_{ci} that at the center of the weak link $\Lambda \gg L$ and the current density is $\boldsymbol{j} = \hat{x} j_x = \hat{x} I/Wd$, where I is the TES current. When the temperature $T > T_{ci}$ and $L \gg \xi(T)$, numerical calculations show that the current density j_x, the order parameter at $x = 0$ in the presence of a current f_0, the order parameter at $x = 0$ in the absence of a current f_{00}, and the gauge-invariant phase difference ϕ across the weak link are accurately related via $f_0/f_{00} = \cos(\phi/2)$ and

$$j_x = j_c \sin\phi = 2j_c(f_0/f_{00})\sqrt{1-(f_0/f_{00})^2}. \qquad (1)$$

The dependence of j_x upon ϕ is similar to that in a Josephson junction.[24] The critical current density, the maximum supercurrent density that can be carried by the weak link, occurs when $\phi = \pi/2$ and $f_0 = f_{00}/\sqrt{2}$. Figure 5 shows j_x/j_c and ϕ/π as functions of f_0/f_{00}.

The GL equations also yield

$$I_c = j_c L d = (F/\xi) e^{-L/\xi}, \qquad (2)$$

where the factor $F = \phi_0 L d f_r^2/3\pi\mu_0\lambda_r^2$ is nearly independent of T for temperatures well below the transition temperature of the leads.

Inferring $T_{ci} = 170.9$ mK from the experimental data in Fig. 2(b) for $L = 290$ μm and assuming $\kappa = \lambda_r/\xi_i$, we obtained $\xi_i = 738$ nm and $\lambda_r = 79$ nm by fitting the

experimental I_c data for $L = 8$ μm at 250 mK and 375 mK. The dotted curves in Fig. 2 show I_c vs T using no additional fitting parameters. The fitted values of ξ_i and λ_r are of the same order of magnitude as corresponding quantities that can be calculated theoretically[27] in the dirty limit for the superconducting part of the bilayers. However, a theory for calculating ξ_i and λ_r accounting for the bilayer proximity effect remains to be developed.

The agreement between the theoretical and experimental curves shown in Fig. 1 is very good except at the lowest critical currents, where we believe thermal rounding effects, not accounted for in the GL theory, are playing a role. Since TESs share some properties with Josephson junctions, it seems likely that when the Josephson coupling energy $\hbar I_c/2e$ drops to values close to $k_B T$, the onset of a voltage as a function of current may well be described by a theory similar to that describing thermal effects in Josephson junctions.[28,29]

Under conditions for which Eq. (2) is valid, if we define the effective transition temperature $T_c(I)$ as the temperature at which the first voltage appears, we can solve for $T_c(I)$ or $t_c = T_c(I)/T_{ci}$ by setting $I = I_c$ in Eq. (2), noting that $\xi = \xi_i/\sqrt{t-1}$. The result is

$$(T_c - T_{ci})/T_{ci} = (\xi_i/L)^2 \ln^2[F\sqrt{t_c - 1}/(I\xi_i)]. \qquad (3)$$

Since the dependence upon t_c on the right-hand side is very weak, Eq. (3) predicts that the current-dependent transition temperature of the TES should scale very nearly as $T_c - T_{ci} \propto 1/L^2$, as observed experimentally. Similar reasoning leads to the conclusion that $\Delta T_{c\,1}$, $\Delta T_{c\,2}$, and ΔT_R also scale as $1/L^2$.

We conclude that TESs behave as weak links. This conclusion is based on our experimental findings that (a) the critical current at the first onset of a voltage along the length depends exponentially upon the length L and the square root of the temperature difference $T - T_{ci}$, (b) both the current-dependent effective transition temperature T_c and the transition width scale as $1/L^2$, and (c) the TESs show clear Fraunhofer-like oscillations as a function of applied magnetic field, similar those in Josephson weak links. It follows that the strength of the superconducting order parameter is not uniform over the TES. Our findings have important implications for TES magnetic field sensitivity, which impacts required limits on ambient magnetic field magnitude and fluctuations in TES applications. Proposed uses of the longitudinal proximity effect for TES applications include (1) tuning the effective T_c of TES arrays by changing L in mask design, which could compensate for bilayer T_{ci} variability[1] and increase yield, and (2) making small TESs consisting of superconducting leads separated by normal metal, such as Au with $T_{ci} = 0$, avoiding the use of S/N bilayers.

Our work at Goddard was partially funded under NASA's Solar and Heliospheric Physics Supporting Research and at the Ames Laboratory by the Department of Energy - Basic Energy Sciences under Contract No. DE-AC02-07CH11358. We thank J. Beyer (PTB Berlin) and K. Irwin (NIST Boulder) for providing the SQUIDS used in this work. We also thank F. Finkbeiner, R. Brekosky, and D. Kelly for essential roles in device fabrication, and C. Kilbourne, I. Robinson, F. S. Porter, R. Kelley, and M. Eckart for useful discussion of these results and the manuscript.

* john.e.sadleir@nasa.gov

1 K. D. Irwin and G. C. Hilton, in *Topics in Applied Physics: Cryogenic Particle Detection*, edited by C. Enss, (Springer, Berlin, 2005).

2 J. M. Martinis, G. C. Hilton, K. D. Irwin, and D. A. Wollman, Nucl. Instrum. Methods. A **444**, 23 (2000).

3 A. Luukanen *et al.*, Phys. Rev. Lett. **90**, 238306 (2003).

4 M. A. Lindeman *et al.*, Nucl. Instrum. Methods. A **559**, 715 (2006).

5 G. W. Fraser, Nucl. Instrum. Methods. A **523**, 234 (2004).

6 G. M. Seidel and I. S. Beloborodov, Nucl. Instrum. Methods. A **520**, 325 (2004).

7 We follow the notation of Likharev[9] and denote the weak link as N′ for $T > T_{ci}$ or S′ for $T < T_{ci}$.

8 J. Clarke, Proc. R. Soc. London. A **308**, 447 (1969).

9 K. K. Likharev, Rev. Mod. Phys. **51**, 101 (1979).

10 J. G. Shepherd, Proc. R. Soc. London. A **326** 421 (1972).

11 S. R. Bandler *et al.*, J. Low Temp. Phys. **151**, 400 (2008).

12 M. K. Bacrania *et al.*, IEEE Trans Nuc. Sci. bf 56, 2299 (2009).

13 J. N. Ullom, J. Low Temp. Phys. **151**, 746 (2008).

14 G. C. Hilton *et al.*, Nature **391**, 672 (1998).

15 S. Friedrich, J. Synchrotron Rad. **13**, 159 (2006).

16 F. S. Porter *et al.*, J. Low Temp. Phys. **151**, 1061 (2008).

17 C. Z. Peng *et al.*, Phys. Rev. Lett. **98**, 010505 (2007).

18 D. Rosenberg *et al.*, Phys. Rev. Lett. **98**, 010503 (2007).

19 D. S. Akerib *et al.*, Phys. Rev. D **72**, 052009 (2005).

20 D. Benford, H. Moseley, and J. Zmuidzinas, J. Phys.: Conf. Ser. **155** 012001(2009).

21 R. L. Kelley *et al.*, AIP Conf. Proc. **1185**, 753 (2009).

22 Measurements of identical TESs but using Mo/Nb leads with either T_c= 3.5 K or 7.1 K were indistinguishable.

23 J. A. Chervenak *et al.*, Nucl. Instrum. Methods. A **520**, 460 (2004).

24 A. Barone and G. Paterno, *Physics and Applications of the Josephson Effect*, (Wiley, New York, 1982).

25 M. Moshe, V. G. Kogan, and R. G. Mints, Phys. Rev. B **78**, 020510 (2008).

26 J. Pearl, Appl. Phys. Lett. **5**, 65 (1964).

27 D. Saint-James, E. J. Thomas, and G. Sarma, *Type II Superconductivity* (Pergamon, Oxford, 1969).

28 Yu. M. Ivanchenko and L. A. Zil'berman, Zh. Eksp. Teor. Fiz. **55**, 2395 (1968) [Sov. Phys. JETP **28**, 1272 (1969)].

29 V. Ambegaokar and B. I. Halperin, Phys. Rev. Lett. **22**, 1364 (1969); erratum: Phys. Rev. Lett. **23**, 274 (1969).